Langmuir

Article

pubs.acs.org/Langmuir

Formic Acid-Assisted Synthesis of Palladium Nanocrystals and Their Electrocatalytic Properties

Qinchao Wang,[†,‡] Yiqian Wang,[†] Peizhi Guo,*[,†,‡] Qun Li,[†,‡] Ruixue Ding,[†,‡] Baoyan Wang,[†,‡] Hongliang Li,[†,‡] Jingquan Liu,[†,‡] and X. S. Zhao[†,‡,§]

[†]State Key Laboratory Breeding Base of New Fiber Materials and Modern Textile, Collaborative Innovation Center for Marine Biomass Fibers, Materials and Textiles of Shandong Province, Qingdao University, Qingdao 266071, P. R. China

[‡]School of Chemistry, Chemical Engineering and Environment, Qingdao University, Qingdao 266071, P. R. China

[§]School of Chemical Engineering, The University of Queensland, St Lucia, QLD 4072, Australia

Supporting Information

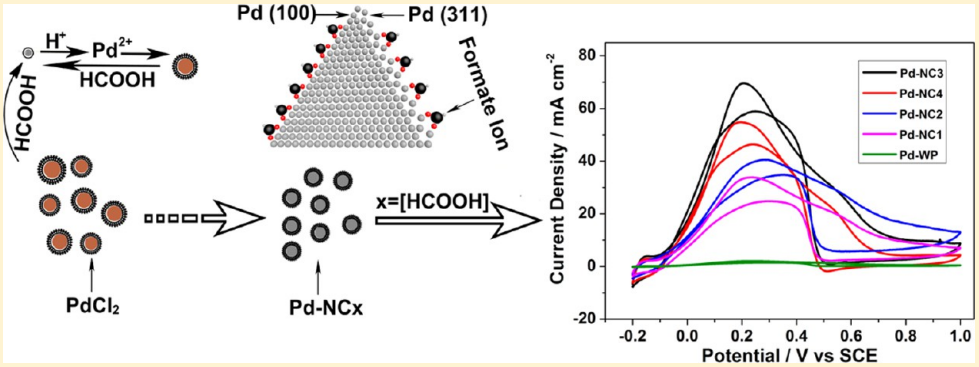

ABSTRACT: Palladium (Pd) nanocrystals have been synthesized by using formic acid as the reducing agent at room temperature. When the concentration of formic acid was increased continuously, the size of Pd nanocrystals first decreased to a minimum and then increased slightly again. The products have been investigated by a series of techniques, including X-ray diffraction, high-resolution transmission electron microscopy (HRTEM), UV−vis absorption, and electrochemical measurements. The formation of Pd nanocrystals is proposed to be closely related to the dynamical imbalance of the growth and dissolution rate of Pd nanocrystals associated with the adsorption of formate ions onto the surface of the intermediates. It is found that small Pd nanocrystals showed blue-shifted adsorption peaks compared with large ones. Pd nanocrystals with the smallest size display the highest electrocatalytic activity for the electrooxidation of formic acid and ethanol on the basis of cyclic voltammetry and chronoamperometric data. It is suggested that both the electrochemical active surface area and the small size effect are the key roles in determining the electrocatalytic performances of Pd nanocrystals. A "dissolution−deposition−aggregation" process is proposed to explain the variation of the electrocatalytic activity during the electrocatalysis according to the HRTEM characterization.

1. INTRODUCTION

Noble metal nanocrystals (NCs) have attracted extensive interest because of their superior optical, magnetic, and catalytic properties compared with the properties of their bulk materials.[1,2] Noble metal NCs have been synthesized with controlled size and shape through the rational design of synthetic systems. In particular, great effort has been devoted to synthesize palladium (Pd) NCs for varied applications, such as electrocatalysis,[3,4] Suzuki coupling reactions,[5,6] automotive exhaust purification,[7] and hydrogen storage.[8,9] Various Pd nanostructures have been prepared by proper synthetic protocols, including hydrothermal synthesis, template method, electrochemical deposition, galvanic replacement, and hemolysis.[10] The electrocatalysis of Pd NCs toward liquid molecules has been studied extensively because of the commercial demand for direct liquid fuel cells.[11]

Platinum (Pt)-based electrocatalysts are prone to being affected by the poison of CO-like intermediates during the electrooxidation process, which obstructs their potential applications. Pd, relatively more abundant in nature and less expensive than Pt, has desirable electrochemical activity toward the electrocatalysis of formic acid and alcohol,[7,8,12] which can be considered as an important candidate of non-Pt electrocatalysts. As the catalytic activity of NCs strongly depends on their size, shape, and surface atomic arrangement,[13−16] great effort has been devoted to synthesize Pd NCs with controlled morphology and size.[17−26] For example, ultrathin hexagonal Pd nanosheets were prepared by using CO as the surface-confining

Received: November 4, 2013
Revised: December 25, 2013
Published: December 25, 2013

agent under a mild condition.[24] Pd NCs with various shapes, including octahedron, cube, decahedron, icosahedron, and nanorods, have been synthesized by using liquid phase synthetic methods.[17−23] An electrochemical method has also been employed to prepare Pd nanorods,[20] tetrahexahedral NCs,[22] and nanospheres.[24] It is well-accepted that the electrooxidation of formic acid has usually been used as an important approach to evaluate the electrocatalytic performance of Pd NCs.[27−30] In fact, Pd nanoparticles can display catalytic activity for the decomposition of formic acid directly in aqueous solutions.[16] However, formic acid also has reducing ability, which may induce the synthesis of Pd from Pd(II) ions.[31] In this regard, the synergistic effect of formic acid on the synthesis of Pd nanostructures and the electrocatalytic feature of Pd nanostructures still need to be further elucidated.

Herein, we report the synthesis of size-tunable Pd NCs by using formic acid as a reducing agent in the presence of polyvinylpyrrolidone (PVP). During the synthetic process, the size of Pd samples was first decreased and later increased gradually, as a result of the imbalance of Pd growth and the dissolution rate, which was proposed to be affected by the dynamical adsorption of formate ions onto the index planes of Pd intermediates. It was found that Pd NCs showed size-dependent optical properties based on the results of UV−vis absorption spectra. The electrochemical activity increased significantly with a slight decrease in the size of Pd NCs. The size of Pd NCs also increased obviously after the electrocatalytic process based on the high-resolution transmission electron microscopy (HRTEM) observations. It was suggested that Pd electrocatalysts should undergo a "dissolution−deposition−aggregation" process during electrocatalysis.

2. EXPERIMENTAL SECTION

2.1. Materials. Palladium(II) chloride, formic acid, sulfuric acid, ethanol, potassium hydroxide, aluminum foil, cetyltrimethylammonium bromide (CTAB), and sodium dodecyl sulfate (SDS) were purchased from Sinopharm Chemical Reagent Co., Ltd. Polyvinylpyrrolidone (PVP) (molecular weight of 58000) was purchased from Acros. All chemicals were analytical grade and used without further purification. Doubly distilled water was used in the experiments.

2.2. Synthesis of Pd NCs. In a typical synthesis, $PdCl_2$ (20 mg), PVP (30 mg), and doubly distilled water (10 mL) were added to a 25 mL beaker while being stirred at room temperature. Formic acid was then quickly added to the mixture. The mixture was stirred for 2 h, and the ultimate black products were collected by centrifugation, washed several times with doubly distilled water and ethanol, and finally dried in an oven at 60 °C for 6 h.[32] The concentration of formic acid in the starting synthetic solutions was set at 1, 2, 3, and 4 M, and the corresponding Pd products were named as Pd-NC1, Pd-NC2, Pd-NC3, and Pd-NC4, respectively. Sample Pd-WP was obtained from the same synthetic system for Pd-NC3 just without PVP. The reaction between palladium chloride and formic acid obeys eq 1:[33]

$$PdCl_2 + HCOOH \rightarrow Pd\downarrow + 2HCl + CO_2\uparrow \quad (1)$$

2.3. Characterization. X-ray diffraction (XRD) experiments were performed on a Bruker D8 Advance X-ray diffractometer equipped with graphite-monochromatized Cu Kα radiation (λ = 0.15418 nm) from 10° to 80° (2θ) using a solid detector. TEM and high-resolution TEM (HRTEM) images were obtained on a JEOL 2100-FEG transmission electron microscope operating at 300 kV. UV−vis absorption spectra were recorded using ethanol solutions (0.1 mg/mL) with a TU1901 UV−vis spectrometer (Beijing Purkinje General Instrument Co., Ltd.). Dynamic light scattering (DLS) experiments were conducted using the Brookhaven laser light scattering system with a BI-200SM research goniometer. A 200 mW green laser (λ = 532 nm) with variable intensity was used, and measurements were taken at room temperature with a scattering angle of 90°. The DLS measurements were taken with dilutions. The average radius and polydispersity index were calculated from the intensity autocorrelation data with the cumulants method.[34]

2.4. Electrochemical Measurements. All the electrochemical measurements were conducted on a CHI760d working station in a three-electrode cell at room temperature. A platinum foil was used as the counter electrode and a saturated calomel electrode (SCE) for the acidic solution or an Hg/HgO electrode for alkaline solutions as the reference electrode. Pd NC-modified glass carbon electrodes (Pd-GCEs) were employed as the working electrodes. After ultrasonication of ethanol suspensions of Pd NCs (1.0 mg/mL) for 1 h, a 10 μL aliquot of the electrocatalyst suspensions was uniformly cast onto the surface of the GCE. Cyclic voltammetry (CV) measurements were taken in 1 M H_2SO_4 solutions at a sweep rate of 100 mV/s at room temperature. CV curves of the electrooxidation of formic acid were recorded in aqueous solutions of 0.5 M H_2SO_4 containing 0.25 M HCOOH. For CV data of ethanol oxidation, the electrolytes were aqueous 1 M CH_3CH_2OH and 1 M KOH solutions.

3. RESULTS AND DISCUSSION

3.1. XRD Analysis. On the basis of the XRD patterns of the products (Figure 1), pure palladium phases were formed for

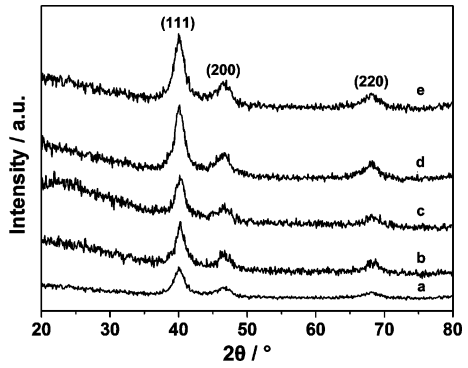

Figure 1. XRD patterns of samples Pd-WP (a), Pd-NC1 (b), Pd-NC2 (c), Pd-NC3 (d), and Pd-NC4 (e).

samples Pd-NC1, Pd-NC2, Pd-NC3, Pd-NC4, and Pd-WP. Three diffraction peaks at 2θ values of 40.3°, 46.7°, and 68.3° can be observed clearly for these samples, which belonged to (111), (200), and (220) planes, respectively, of the cubic phase of palladium (JCPDS PDF 46-1043). The broad diffraction peaks indicated the formation of small crystals in the products. The average sizes of Pd particles were in the following order: Pd-WP > Pd-NC1 > Pd-NC2 > Pd-NC4 > Pd-NC3 [calculated from the strongest peak of the (111) plane in Figure 1 (Supporting Information) based on the Scherrer equation].[21]

3.2. TEM and HRTEM Studies. Figure 2 shows the TEM and HRTEM images of all the Pd NCs. It can be seen that small nanoparticles were formed for all the Pd NCs except Pd-WP (Figure S1 of the Supporting Information). On the basis of the particle size distributions (the inset columnar profiles in Figure 2), the average sizes of Pd-NC1, Pd-NC2, Pd-NC3, and Pd-NC4 were approximately 5.7, 4.5, 4.1, and 4.3 nm, respectively, the same tendency as that obtained from the XRD results (Figure 1). Furthermore, the higher the concentration of formic acid in the synthetic systems, the narrower the distribution of the particle size. As depicted in the top-right insets in panels A, C, E, and G of Figure 2, the selected-area electron diffraction (SAED) patterns of Pd NCs indicated the crystalline nature of all the samples. Furthermore, HRTEM images (Figure 2B,D,F,H) of individual Pd NCs

dx.doi.org/10.1021/la404268j | Langmuir 2014, 30, 440−446

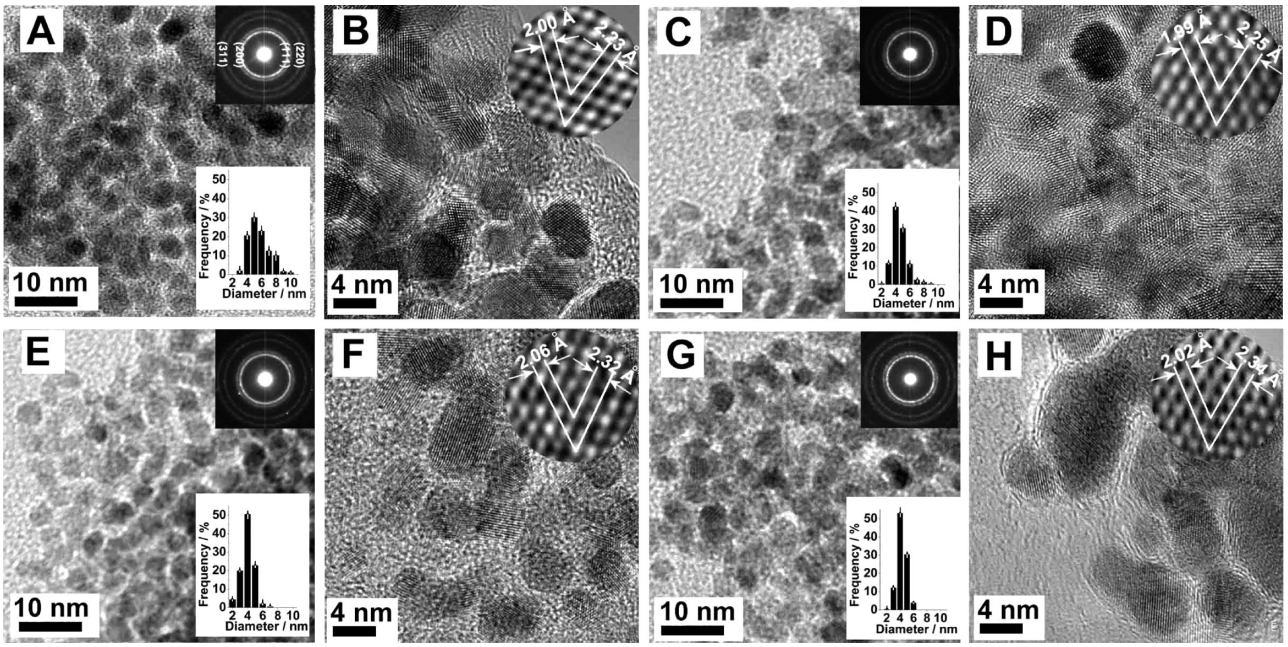

Figure 2. TEM (A, C, E, and G) and HRTEM (B, D, F, and H) images of Pd-NC1 (A and B), Pd-NC2 (C and D), Pd-NC3 (E and F), and Pd-NC4 (G and H). Each of the particle size distribution profiles was derived from ~250 NCs. The diameter of all the inset HRTEM images in panels B, D, F, and H was set to 2 nm.

confirmed the single-crystalline nature. The interplanar spacings of the lattice fringes of Pd NCs were 1.99−2.06 and 2.23−2.34 Å, ascribed to the (200) and (111) lattice planes of cubic Pd, respectively. The angle between the crystalline planes was ~53.2° (the insets in Figure 2B,D,F,H), which closely matched the theoretical value.[36] Thus, the zone axis should be the (110) facets based on the results described above.

3.3. UV−Vis Absorption Spectra. The UV−vis absorption properties of Pd NCs were measured, as shown in Figure 3. All

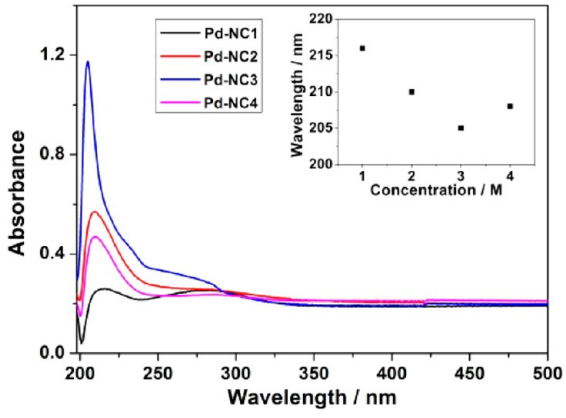

Figure 3. UV−vis absorption spectra of Pd nanoparticles in ethanol solutions (0.1 mg/mL). The inset shows the variation of the peak position of Pd nanoparticles with formic acid concentration in the synthetic solutions.

the Pd NPs showed obvious absorption peaks in the ultraviolet region. The sharp extinction peaks were observed at 212, 210, 205, and 208 nm, assigned to surface plasmon resonance (SPR)[21,35] for Pd-NC1, Pd-NC2, Pd-NC3, and Pd-NC4, respectively. Clearly, the absorption peak was blue-shifted with the slight decrease in the size of Pd NCs,[21,24,36] and the smallest Pd-NCs showed the strongest intensity under the same condition among all the measured samples. Besides, a weak peak that appeared at ~280 nm was also obtained for all the samples possibly because of the formation of loose nanoparticle clusters based on the DLS results (Figure S2 of the Supporting Information).

3.4. Evolution of the Intermediates. To study the mechanism of formation of Pd NCs, intermediary products of all the synthetic systems were collected at every 20 min interval during the synthetic process. It should also be noted that Pd samples cannot be obtained until the reaction time reached 60 min. The intermediates, collected from the synthetic system for Pd-NC3 as an example, were characterized by XRD (Figure S3 of the Supporting Information). It can be derived from Figure S3 of the Supporting Information that the sizes of the precipitates decreased with synthetic time from 60 to 100 min. However, further increasing the reaction time to ~120 min afforded the smallest particles. The particle size was then increased when the synthetic time was further prolonged. Similar results can also be indirectly derived from the physicochemical properties of Pd intermediates obtained from all the reaction mixtures based on the corresponding results of UV−vis absorption spectra (Figure S4 of the Supporting Information) and electrochemical measurements (Figure 4 and Figure S5 of the Supporting Information). Therefore, the reaction time was fixed at 2 h for the synthesis of the targeted Pd NCs.

It was interesting to note that many bubbles were generated immediately when our Pd NCs were added to formic acid solutions. In the meantime, the color of the solution gradually changed to slight yellow, indicating the formation of Pd(II) ions (Supporting Information). If Pd NCs were immersed in 3 M formic acid solutions for 6 h, an ~40% weight loss was observed. The residual Pd particles were larger than the original ones as derived from the XRD patterns (Figure S6 of the Supporting Information) because of the dual effects of formic acid as both the weak acid and reducing agent.

dx.doi.org/10.1021/la404268j | Langmuir 2014, 30, 440−446

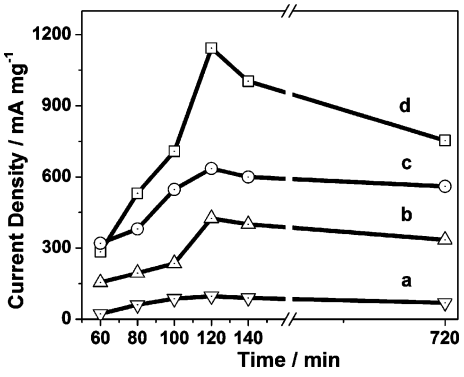

Figure 4. Variation of current densities for the positive scan in CV curves of the intermediates from the synthetic systems for Pd-NC1 (a), Pd-NC2 (b), Pd-NC3 (d), and Pd-NC4 (c) performed in 1 M KOH/1 M CH_3CH_2OH media with potential window ranges from −0.85 to 0.30 V.

On the basis of the results given above, the mechanism of formation of Pd NCs was proposed as shown in Figure 5. At

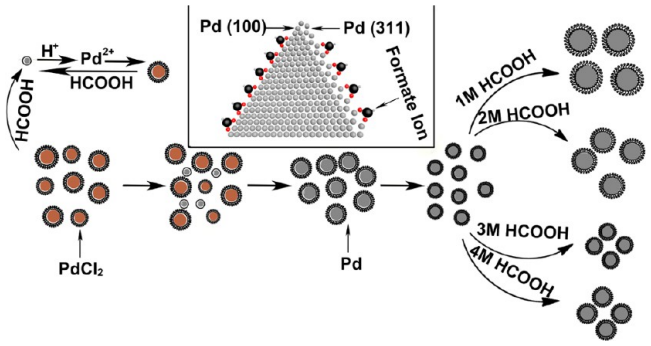

Figure 5. Schematic illustration of the mechanism of formation of Pd NCs. The inset is an illustration of the absorption of formate ions on Pd (100) and (311) facets.

the beginning, $PdCl_2$ particles tended to react with formic acid to afford small ones, during which PVP worked as a surfactant to prevent aggregation.[37] Pd(II) ions were reduced by formic acid, and Pd particles were formed. Subsequently, Pd crystal nuclei or small particles can also become Pd(II) ions because of the weak acidic environment as well as the strong reactive ability of Pd nuclei. The reaction between formic acid and Pd can be dynamically adjusted by changing both the concentration of formic acid and the structure of Pd nuclei. With the elongation of the synthesis time, smaller particles were obtained. When the reduction of Pd(II) ions was quicker than the oxidization of Pd particles, the particle size was increased. Increasing the concentration of formic acid enhanced the acidity of the solution, promoting the dissolution of small Pd particles. These should contribute to the formation of the smallest NCs under the 3 M formic acid system. During the synthetic process, the adsorption of formate ions is thought to occur on the (100) terrace with two oxygen atoms linked to the bridge sites of (100) on the crystalline surfaces.[38] In the meantime, formate ions can also attached to the step line of Pd (311) facets.[39] With a concentration of formic acid of ≤4 M, more formate ions could be adsorbed on the surface of Pd (100) and (311) facets, which retarded the reaction of small Pd particles, leading to the slight increase in particle size.

It should also be pointed out that the concentration of $PdCl_2$ in the synthetic solutions and the types of surfactants can affect the synthesis of Pd NCs. In the experiments described above, the concentration of $PdCl_2$ in the reaction solutions was 2 mg/mL. If the $PdCl_2$ concentration was changed to 1 or 4 mg/mL, the obtained Pd samples were larger and had lower electrochemical activity than Pd-NC3 with the original $PdCl_2$ concentration of 2 mg/mL (Figures S7 and S8 of the Supporting Information). When CTAB or SDS was used as the surfactant under similar conditions, >20 nm Pd particles were formed (Figure S9 of the Supporting Information), and they displayed weaker electrocatalytic performance than Pd-NC3 (Figure S10 of the Supporting Information). This should be ascribed to the reason that PVP molecules chemisorb with both oxygen and nitrogen atoms in the ring on the surfaces of large Pd nanoparticles, which would restrict the growth of Pd nanocryatals.[40]

3.5. Electrochemical Studies. Figure 6 shows the cyclic voltammograms (CVs) for the Pd NC-modified glass carbon

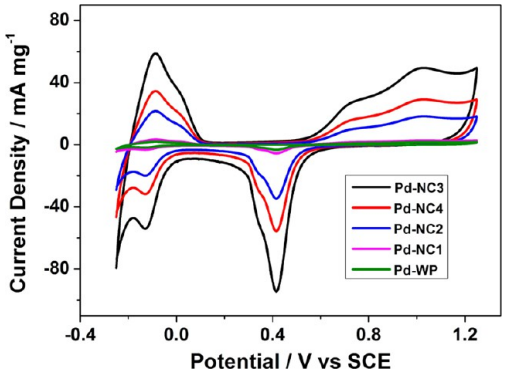

Figure 6. CV curves of Pd-GCEs in aqueous H_2SO_4 (1 M) solutions.

electrodes (Pd-GCEs) in an aqueous H_2SO_4 (1 M) electrolyte at a scan rate of 100 mV/s. The CV curves of Pd-GCEs were quite different from that of the naked GCE, which were typical for Pd-modified electrodes.[24] A sharp peak at 0.410 V (vs SCE) can be attributed to the reduction peak of produced Pd oxide.[27] Besides, the two peaks that appeared at −0.088 and 0.018 V (vs SCE) in the positive sweep are widely considered as the adsorption of hydrogen in the surface of Pd particles, which are usually used to estimate the electrochemically active surface area (ECSA).[24,32,41,42] The ECSAs of Pd-NC1-, Pd-NC2-, Pd-NC3-, Pd-NC4-, and Pd-WP-modified electrodes were calculated to be 1.30, 3.22, 4.49, 3.49, and 0.64 cm^2/mg, respectively, based on the formula $Q(\mu C)/424\ cm^2$, in which Q stands for the corresponding electrical quantity of the inflection point according to the integral of the reduction peak.[32,41,42] This is a standard electrochemical method frequently used for determining the ECSA of Pd nanoparticles.

The electrocatalytic properties of Pd NCs and Pd-WP toward the electrooxidation of formic acid and ethanol have been investigated (Figures 7 and 8). Clearly, all the Pd NCs exhibited higher electrocatalytic activity than Pd-WP. Furthermore, the order of electrocatalytic performance of Pd samples is as follows: Pd-WP < Pd-NC1 < Pd-NC2 < Pd-NC4 < Pd-NC3. We can also conclude from Figures 7 and 8 that not only the ECSA but also the particle size of Pd NCs can contribute to the electrocatalytic performance of Pd samples. With the highest ECSA and the smallest size among all the Pd

dx.doi.org/10.1021/la404268j | Langmuir 2014, 30, 440−446

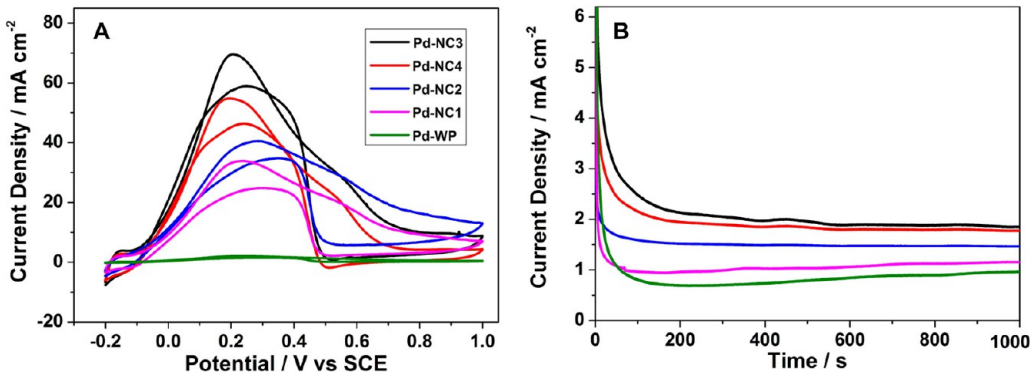

Figure 7. (A) CV curves of Pd-GCEs in 0.25 M HCOOH/0.5 M H_2SO_4 solutions at 50 mV/s and (B) chronoamperometric curves of Pd-GCEs at 0.3 V.

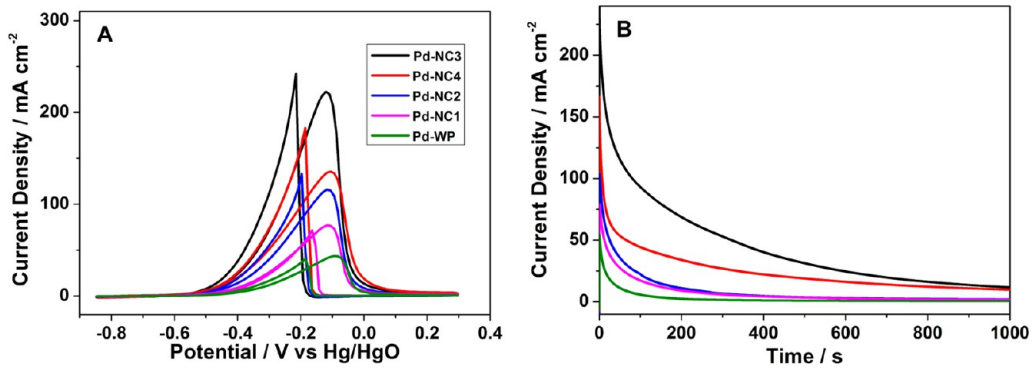

Figure 8. (A) CV curves of Pd-GCEs in 1 M C_2H_5OH/1 M KOH solutions at 50 mV/s and (B) chronoamperometric curves of Pd-GCEs at 0.3 V.

NCs, Pd-NC3 showed the highest catalytic density toward the electrooxidation of formic acid and ethanol.[20,43,44]

For Pd-NC3-GCE, the current densities were 70 and 61 mA/cm^2 in the formic acid electrolyte for the positive and negative scans, respectively. This observed difference may be induced by adsorption of intermediate products that was produced during the oxidation of formic acid.[6,45−48] Furthermore, the onset potential of Pd-NC3-GCE tended to be more negative than those of other modified GCEs (Figures 7A and 8A), indicating the best electrocatalytic oxidation activity of Pd-NC3. The ratio of the forward to backward current intensities of Pd-NC3 is also higher than that of Pd-NC4, which indicated the CO tolerance of Pd-NC3 was better than that of Pd-NC4.[49−51] Chronoamperometric data (Figure 7B) showed that the current density decreased quickly with time and reached a plateau after ∼100 s for all the Pd-GCEs, in which the order for the electrooxidation of formic acid can be observed to be the same as that derived from Figure 6A.

As depicted in Figure 8A, Pd-NC3-GCE also exhibited the highest catalytic current densities of 222 and 254 mA/cm^2 for the positive and negative scans for the electrooxidation of ethanol, respectively, among all the Pd-GCEs. These were higher than those of commercial Pd and Pd/C samples (Figure S11 of the Supporting Information). Figure 8B shows transient current densities for ethanol oxidation of Pd-GCEs, which decreased slowly compared with those for formic acid oxidation (Figure 7B). Especially for Pd-NC3-GCE, the current density decreased rapidly only in the first 40 s and then decreased slowly until 700 s had passed. Finally, a proximate plateau was observed. This may be ascribed to the factors of catalyst, increased viscosity of the solutions, and the decreased concentration of H^+ or OH^- ions.[10] Besides, the competitive adsorption of the substrate/partial oxidation product on the catalyst surface may lower the efficiency of the reaction rate.[10] Furthermore, the alkaline employed in ethanol oxidation reduced the risk of corrosion of the metal catalyst, which may retard Pd inactivation.[52] This can be verified by the electrocatalytic stability against cycle number of Pd-GCEs toward the electrooxidation of ethanol, as shown in Figure S12 of the Supporting Information. It can be seen that all electrodes can reach the highest current density within 20 cycles and decrease obviously after 60 cycles. Clearly, Pd-NC3-GCE displayed the highest electrocatalytic stability among all the Pd-GCEs.

The structural change of Pd-NC3 after the electrocatalysis of formic acid (Pd-NC3B) (100 cycles) was investigated by HRTEM (Figure 9). As shown in Figure 9A, the average size of Pd-NC3B was ∼6 nm larger than that of Pd-NC3. Figure 9B shows the enlarged image of the boxed area in Figure 9A. It was found that the crystal phase and lattice spacing were unchanged during the variation of the morphology (Figures 2F and 9B). However, aggregation of Pd-NC3B can be observed clearly when compared with Pd-NC3 (Figure 2E,F). It was suggested that Pd NCs should undergo a dissolution−deposition−aggregation process during electrocatalysis, as illustrated at the bottom right of Figure 9. The formation of large Pd nanoparticles may be ascribed to the Ostwald ripening effect because large particles have low surface energy and reaction activity.[45] Consequently, Pd-NC3B showed electrochemical activity lower than that of Pd-NC3.

dx.doi.org/10.1021/la404268j | *Langmuir* 2014, 30, 440−446

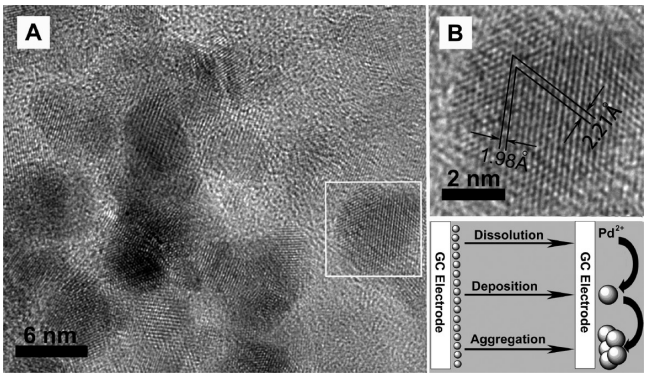

Figure 9. Typical HRTEM images (A) of Pd NC3B. Panel B is the white rectangular area in panel A. The image at the bottom right is an illustration of the variation of Pd NCs during electrocatalysis.

4. CONCLUSION

Pd nanocrystals with tunable sizes were synthesized at room temperature by adjusting the concentration of formic acid in the synthetic systems. The formation of Pd nanocrystals was attributed to the dynamic regulation of the dissolution and growth of Pd intermediates during the synthetic process. It is found that the absorption peak was gradually blue-shifted with the continuous decrease in the size of Pd nanocrystals. Furthermore, smaller Pd nanocrystals display higher electrocatalytic activity for the electrooxidation of formic acid and ethanol than the large ones. The strong electrocatalytic performance of Pd nanocrystals should be ascribed to both the large electrochemically active surface area and small size effect of the samples. It was found that irregular large particles were formed after the electrocatalytic process because of the dissolution−deposition−aggregation process. These results pave the way for the development of new Pd nanostructures based on the rational design of synthetic systems.

■ ASSOCIATED CONTENT

Ⓢ Supporting Information

Figures S1−S12. This material is available free of charge via the Internet at http://pubs.acs.org.

■ AUTHOR INFORMATION

Corresponding Author

*E-mail: pzguo@qdu.edu.cn or guopz77@yahoo.com. Telephone: +86 532 8595 1290. Fax: +86 532 8595 5529.

Notes

The authors declare no competing financial interest.

■ ACKNOWLEDGMENTS

This work is financially supported by the National Natural Science Foundation of China (21143006 and U1232104), the National High Technology Research and Development Program of China (2012AA110407), the Foundation of Qingdao Municipal Science and Technology Commission [11-2-4-2-(8)-jch], and the Foundation of "Taishan Scholar" program of Shandong Province, P. R. China.

■ REFERENCES

(1) Burda, C.; Chen, X. B.; Narayanan, R.; El-Sayed, M. A. Chemistry and Properties of Nanocrystals of Different Shapes. *Chem. Rev.* **2005**, *105*, 1025−1102.

(2) Gonzalez, E.; Arbiol, J.; Puntes, V. F. Carving at the Nanoscale: Sequential Galvanic Exchange and Kirkendall Growth at Room Temperature. *Science* **2011**, *334*, 1377−1380.

(3) Tian, N.; Zhou, Z. Y.; Sun, S. G.; Ding, Y.; Wang, Z. L. Synthesis of Tetrahexahedral Platinum Nanocrystals with High-Index Facets and High Electro-Oxidation Activity. *Science* **2007**, *316*, 732−735.

(4) Jin, M. S.; Zhang, H.; Xie, Z. X.; Xia, Y. N. Palladium Concave Nanocubes with High-Index Facets and Their Enhanced Catalytic Properties. *Angew. Chem., Int. Ed.* **2011**, *50*, 7850−7858.

(5) Garcia-Martinez, J. C.; Lezutekong, R.; Crooks, R. M. Dendrimer-Encapsulated Pd Nanoparticles as Aqueous, Room-Temperature Catalysts for the Stille Reaction. *J. Am. Chem. Soc.* **2005**, *127*, 5097−5103.

(6) Chtchigrovsky, M.; Lin, Y.; Ouchaou, K.; Chaumontet, M.; Robitzer, M.; Quignard, F.; Taran, F. Dramatic Effect of the Gelling Cation on the Catalytic Performances of Alginate-Supported Palladium Nanoparticles for the Suzuki-Miyaura Reaction. *Chem. Mater.* **2012**, *24*, 1505−1510.

(7) Nishihata, Y.; Mizuki, J.; Akao, T.; Tanaka, H.; Uenishi, M.; Kimura, M.; Okamoto, T.; Hamada, N. Self-Regeneration of a Pd-Perovskite Catalyst for Automotive Emission Control. *Nature* **2002**, *418*, 164−167.

(8) Xu, C. W.; Wang, H.; Shen, P. K.; Jiang, S. P. Highly Ordered Pd Nanowire Arrays as Effective Electrocatalysts for Ethanol Oxidation in Direct Alcohol Fuel Cells. *Adv. Mater.* **2007**, *19*, 4256−4259.

(9) Ong, M. D.; Jacobs, B. W.; Sugar, J. D.; Grass, M. E.; Liu, Z.; Buffleben, G. M.; Clift, W. M.; Langham, M. E.; Cappillino, P. J.; Robinson, D. B. Effect of Rhodium Distribution on Thermal Stability of Nanoporous Palladium-Rhodium Powders. *Chem. Mater.* **2012**, *24*, 996−1004.

(10) Bianchini, C.; Shen, P. K. Palladium-Based Electrocatalysts for Alcohol Oxidation in Half Cells and in Direct Alcohol Fuel Cells. *Chem. Rev.* **2009**, *109*, 4183−4206.

(11) Antolini, E. Palladium in Fuel Cell Catalysis. *Energy Environ. Sci.* **2009**, *2*, 915−931.

(12) Yin, S. B.; Cai, M.; Wang, C. X.; Shen, P. K. Tungsten Carbide Promoted Pd-Fe as Alcohol-Tolerant Electrocatalysts for Oxygen Reduction Reactions. *Energy Environ. Sci.* **2011**, *4*, 558−563.

(13) Crespo-Quesada, M.; Andanson, J.; Yarulin, A.; Lim, B.; Xia, Y. N.; Kiwi-Minsker, L. UV-Ozone Cleaning of Supported Poly(vinylpyrrolidone)-Stabilized Palladium Nanocubes: Effect of Stabilizer Removal on Morphology and Catalytic Behavior. *Langmuir* **2011**, *27*, 7709−7916.

(14) Narayanan, R.; El-Sayed, M. A. Shape-Dependent Catalytic Activity of Platinum Nanoparticles in Colloidal Solution. *Nano Lett.* **2004**, *4*, 1343−1348.

(15) Sharma, S.; Kim, B.; Lee, D. Water-Soluble Pd Nanoparticles Capped with Glutathione: Synthesis, Characterization, and Magnetic Properties. *Langmuir* **2012**, *28*, 15958−15965.

(16) Bratlie, K. M.; Lee, H.; Komvopoulos, K.; Yang, P. D.; Somorjai, G. A. Platinum Nanoparticles Shape Effects on Benzene Hydrogenation Selectivity. *Nano Lett.* **2007**, *7*, 3097−3101.

(17) Fan, F. R.; Attia, A.; Sur, U. K.; Chen, J. B.; Xie, Z. X.; Li, J. F.; Ren, B.; Tian, Z. Q. An Effective Strategy for Room-Temperature Synthesis of Single-Crystalline Palladium Nanocubes and Nanodendrites in Aqueous Solution. *Cryst. Growth Des.* **2009**, *9*, 2335−2340.

(18) Huang, X. Q.; Tang, S. H.; Zhang, H. H.; Zhou, Z. Y.; Zheng, N. F. Controlled Formation of Concave Tetrahedral/Trigonal Bipyramidal Palladium Nanocrystals. *J. Am. Chem. Soc.* **2009**, *131*, 13916−13917.

(19) Wang, Y.; Xie, S. F.; Liu, J. Y.; Park, J.; Huang, C. Z.; Xia, Y. N. Shape-Controlled Synthesis of Palladium Nanocrystals: A Mechanistic Understanding of the Evolution from Octahedrons to Tetrahedrons. *Nano Lett.* **2013**, *13*, 2276−2281.

(20) Tian, N.; Zhou, Z. Y.; Sun, S. G. Electrochemical Preparation of Pd Nanorods with High-Index Facets. *Chem. Commun.* **2009**, 1502−1504.

(21) Li, C. C.; Sato, R.; Kanehara, M.; Zeng, H. B.; Bando, Y.; Teranishi, T. Controllable Polyol Synthesis of Uniform Palladium Icosahedra: Effect of Twinned Structure on Deformation of Crystalline Lattices. *Angew. Chem., Int. Ed.* **2009**, *48*, 6883−6887.
(22) Tian, N.; Zhou, Z. Y.; Yu, N. F.; Wang, L. Y.; Sun, S. G. Direct Electrodeposition of Tetrahexahedral Pd Nanocrystals with High-Index Facets and High Catalytic Activity for Ethanol Electrooxidation. *J. Am. Chem. Soc.* **2010**, *132*, 7580−7581.
(23) Sankar, M.; He, Q.; Morad, M.; Pritchard, J.; Freakley, S. J.; Edwards, J. K.; Taylor, S. H.; Morgan, D. J.; Carley, A. F.; Knight, D. W.; Kiely, C. J.; Hutchings, G. J. Synthesis of Stable Ligand-Free Gold-Palladium Nanoparticles Using a Simple Excess Anion Method. *ACS Nano* **2012**, *6*, 6600−6613.
(24) Huang, X. Q.; Tang, S. H.; Mu, X. L.; Dai, Y.; Chen, G. X.; Zhou, Z. Y.; Ruan, F. X.; Yang, Z. L.; Zheng, N. F. Freestanding Palladium Nanosheets with Plasmonic and Catalytic Properties. *Nat. Nanotechnol.* **2011**, *6*, 28−32.
(25) Erikson, H.; Sarapuu, A.; Alexeyeva, N.; Tammeveski, K.; Solla-Gullon, J.; Feliu, J. M. Electrochemical Reduction of Oxygen on Palladium Nanocubes in Acid and Alkaline Solutions. *Electrochim. Acta* **2012**, *59*, 329−335.
(26) Jin, M. S.; Zhang, H.; Xie, X.; Xia, Y. N. Palladium Nanocrystals Enclosed by {100} and {111} Facets in Controlled Proportions and their Catalytic Activities for Formic Acid Oxidation. *Energy Environ. Sci.* **2012**, *5*, 6352−6357.
(27) Yu, Y.; Zhang, Q. B.; Liu, B.; Lee, J. Y. Synthesis of Nanocrystals with Variable High-Index Pd Facets through the Controlled Heteroepitaxial Growth of Trisoctahedral Au Templates. *J. Am. Chem. Soc.* **2010**, *132*, 18258−18265.
(28) Niu, W. X.; Zhang, L.; Xu, G. B. Shape-Controlled Synthesis of Single-Crystalline Palladium Nanocrystals. *ACS Nano.* **2010**, *4*, 1987−1997.
(29) Niu, Z. Q.; Peng, Q.; Gong, M.; Rong, H. P.; Li, Y. D. Oleylamine-Mediated Shape Evolution of Palladium Nanocrystals. *Angew. Chem., Int. Ed.* **2011**, *50*, 6315−6319.
(30) Dai, Y.; Mu, X. L.; Tan, Y. M.; Lin, K. Q.; Yang, Z. L.; Zheng, N. F.; Fu, G. Carbon Monoxide-Assisted Synthesis of Single-Crystalline Pd Tetrapod Nanocrystals though Hydride Fromation. *J. Am. Chem. Soc.* **2012**, *134*, 7073−7080.
(31) Corradini, P. G.; Antolini, E.; Perez, J. Structural and Electrochemical Characterization of Carbon Supported Pt-Pr Catalysts for Direct Ethanol Fuel Cells Prepared Using a Modified Fomic Acid Method in CO Atmosphere. *Phys. Chem. Chem. Phys.* **2013**, *15*, 11730−11739.
(32) Guo, P. Z.; Wei, Z. B.; Ye, W. N.; Qin, W.; Wang, Q. C.; Guo, X. F.; Lu, C. J.; Zhao, X. S. Preparation and Characterization of Nanostructured Pd with High Electrocatalytic Activity. *Colloids Surf., A* **2012**, *395*, 75−81.
(33) Chen, S. *Important inorganic chemical reactions*, 3rd ed.; Shanghai Science and Technology Press: Shanghai, 1994.
(34) Zhao, C. H.; Tan, J. J.; Li, W.; Tong, K.; Xu, J.; Sun, D. J. Ca^{2+} Ion Responsive Pickering Emulsions Stabilized by PSSMA Nano-aggregates. *Langmuir* **2013**, *29*, 14421−14428.
(35) School, J. A.; Koh, A. L.; Dionnw, J. A. Quantum Plasmon Resonances of Individual Metallic Nanoparticles. *Nature* **2012**, *483*, 421−427.
(36) Buerger, M. J. *Crystal Structure Analysis*; R. E. Krieger Publishing Co.: Huntington, NY, 1980.
(37) Mandal, D.; Kim, K. J.; Lee, J. S. Simple Synthesis of Palladium Nanoparticles, β-Phase Formation, and the Control of Chain and Dipole Orientations in Palladium-Doped Poly(vinylidene Fluoride) Thin Films. *Langmuir* **2012**, *28*, 10310−10317.
(38) Furuya, N.; Koide, S. Hydrogen Adsorption on Platinum Single-Crystal Surfaces. *Surf. Sci.* **1989**, *220*, 18−28.
(39) Hoshi, N.; Kida, K.; Nakamura, M.; Nakada, M.; Osada, K. Structural Effects of Electrochemical Oxidation of Formic Acid on Single Crystal Electrodes of Palladium. *J. Phys. Chem. B* **2006**, *110*, 12480−12484.
(40) Xian, J. Y.; Hua, Q.; Jiang, Z. Q.; Ma, Y. S.; Huang, W. X. Size-Dependent Interaction of the Poly(N-vinyl-2-pyrrolidone) Capping Ligand with Pd Nanocrystals. *Langmuir* **2012**, *28*, 6736−6741.
(41) Bard, A. J., Ed. *Electrochemistry of Elements*; Marcel Dekker, Inc.: New York, 1973; Vol. 9, pp 48−58.
(42) Song, S. Q.; Wang, Y.; Tsiakaras, P.; Shen, P. K. Direct Alcohol Fuel Cells: A novel Non-Platinum and Alcohol Inert ORR Electrocatalyst. *Appl. Catal., B* **2008**, *78*, 381−387.
(43) Li, M.; Guo, W. Y.; Jiang, R. B.; Zhao, L. M.; Shan, H. H. Decomposition of Ethanol on Pd(111): A Density Functional Theory Study. *Langmiur* **2010**, *26*, 1879−1888.
(44) Teranishi, T.; Miyake, M. Size Control of Palladium Nanoparticles and their Crystal Structures. *Chem. Mater.* **1998**, *10*, 594−600.
(45) Miah, M. R.; Alam, M. T.; Okajima, T.; Ohsaka, T. Electrochemically Fabricated Tin-Palladium Bimetallic Electrocatalyst for Oxygen Reduction Reaction in Acidic Media. *J. Electrochem. Soc.* **2009**, *156*, B1142−B1149.
(46) Mazumder, V.; Sun, S. H. Oleylamine-Mediated Synthesis of Pd Nanoparticles for Catalytic Formic Acid Oxidation. *J. Am. Chem. Soc.* **2009**, *131*, 4588−4589.
(47) Jin, Z.; Nackashi, D.; Lu, W.; Kittrell, C.; Tour, J. M. Decoration, Migration, and Aggregation of Palladium Nanoparticles on Graphene Sheets. *Chem. Mater.* **2010**, *22*, 5695−5699.
(48) Yao, Z. Q.; Yue, R. R.; Jiang, F. X.; Zhai, C. Y.; Ren, F. F.; Du, Y. K. Electrochemical-Reduced Graphene Oxide-Modified Carbon Fiber as Pt-Au Nanoparticle Support and its High Efficient Electrocatalytic Activity for Formic Acid Oxidation. *J. Solid State Electrochem.* **2013**, *17*, 2511−2519.
(49) Lamy, C.; Lima, A.; Lerhun, V.; Delime, F.; Coutanceau, C.; Leger, J. M. Recent Advances in the Development of Direct Alcohol Fuel Cells (DAFC). *J. Power Sources* **2002**, *105*, 283−296.
(50) Huang, J. C.; Liu, Z. L.; He, C. B.; Gan, L. M. Synthesis of PtRu Nanoparticles from the Hydrosilylation Reaction and Application as Catalyst for Direct Methanol Fuel Cell. *J. Phys. Chem. B* **2005**, *109*, 16644−16649.
(51) Bambagion, V.; Bianchini, C.; Marchionni, A.; Filippi, J.; Vizza, F.; Teddy, J.; Serp, P.; Zhiani, M. Pd and Pt-Ru Anode Electrocatalysts Supported on Multi-Walled Carbon Nanotubes and their Use in Passive and Active Direct Alcohol Fuel Cells with an Anion-Exchange Membrane (Alcohol = Methanol, Glycerol). *J. Power Sources* **2009**, *190*, 241−251.
(52) Shao, Z. B.; Zhu, W.; Wang, H.; Yang, Q. H.; Yang, S. L.; Liu, X. D.; Wang, G. Z. Controllable Synthesis of Concave Nanocubes, Right Bipyramids, and 5-Fold Twinned Nanorods of Palladium and their Enhanced Electrocatalytic Performance. *J. Phys. Chem. C* **2013**, *117*, 14289−14294.